Journal of the Iranian Chemical Society (2022) 19:3797–3813
https://doi.org/10.1007/s13738-022-02567-y

ORIGINAL PAPER

Synthesis, spectroscopic, electrochemical, thermal and antimicrobial studies of Ni(II), Zn(II), Cu(II) and Co(II) metal complexes of novel bidentate schiff base ligand

Prerna Turk[1,2] · Kiran Singh[1] · Anita Dhanda[3]

Received: 13 October 2021 / Accepted: 8 April 2022 / Published online: 30 April 2022

Abstract
New Schiff base was synthesized from condensation of anthracene-10-carbaldehyde with 4-amino-3-mercapto-1,2,4-triazin-5(4*H*)-one. Resulted azomethine was characterized via elemental analysis, infrared and ^{1}H-NMR spectroscopy. Thereafter, novel Schiff base complexes with Co(II), Ni(II), Zn(II) and Cu(II) metals were prepared and characterized by analytical, conductivity data, proton-NMR, IR, UV–Visible, ESR and fluorescence spectroscopy, magnetic moment as well as cyclic voltammetry. These physicochemical techniques suggest monobasic bidentate behaviour of ligand towards metal ions. Thermal stability and degradation kinetics have been studied using thermogravimetric techniques and some other thermal parameters are also reported. All the complexes exhibit octahedral geometry except copper complexes which show square planar arrangement around the metal centre. Low conductivity data of all compounds reveal their neutral and non-electrolytic character. Antimicrobial potentials of Schiff base and its metal chelates were evaluated against wide spectrum of bacterial cultures such as *P. aeruginosa*, *S. aureus, B. subtilis*, *E. coli* and fungi like *A. niger* and *A. flavus.*

Keywords Antibacterial activity · Fluorescent metal complexes · Thermogravimetric analysis · 4-(anthracen-10-ylmethyleneamino)-3-mercapto-1,2,4-triazin-5(4*H*)-one · Quasi-reversible Cu(II) complexes · Schiff base

Introduction

4-Amino-3-mercapto-1,2,4-triazin-5(4*H*)-one derivatives have been studied due to their herbicidal, antimicrobial and anticancer activities [1]. Many transition metal chelates of Schiff bases having 4-amino-3-mercapto-6-methyl-1,2,4-triazin-5(4*H*)-one have been reported [2–5]. But less work has been done on 4-amino-3-mercapto-1,2,4-triazin-5(4*H*)-one based metal chelates. This kind of compounds have many applications in medicinal, catalytic and industrial field [6, 7]. In coordination chemistry, the chemistry of transition metal complexes having heterocyclic moieties with thione/thiol groups has been an interesting research area in synthetic inorganic chemistry due to their diverse structural features and importance in biological field also.

Anthracene owns an exclusive electron-rich assembly with small electronic bandgap and shows intense blue fluorescence. Thus, it has been employed as a production fragment in diverse emissive objects [8, 9]. Anthracene derivatives are one of the promising structures due to their intensive luminescence properties and high thermal stabilities. Interesting fluorescent properties are revealed by anthracene derivatives [10]. The emission of anthracene derivatives lies in the visible region due to its intermolecular packing and conjugation over the extended area of the aromatic ring. Such conjugated organic moieties having some sort of optoelectronic properties are still of interest in spite of commercialization of such materials. Among such compounds, Schiff bases have been successful in grabbing the attention of researchers. Derivatives of Schiff bases having fluorescent chromophore can be utilized as sensors for metal ion centres. The fluorescent properties and quantum yields of metal complexes get changed with respect to their parent ligand after complexation with different metal ions [11].

✉ Kiran Singh
knsingh@kuk.ac.in; turkprerna23@gmail.com

[1] Department of Chemistry, Kurukshetra University, Kurukshetra, Haryana 136119, India

[2] Government College Bherian, Kurukshetra, Haryana 136119, India

[3] Department of Microbiology, Kurukshetra, University, Kurukshetra, Haryana 136119, India

Medicinal inorganic chemistry has become of great interest since last few decades. Resistance of microbes towards commonly existing antibiotics is causing problems which directs the inorganic researchers to synthesize new antimicrobial compounds to combat these obstinate pathogens. Schiff bases having heterocyclic aromatic moieties have been proved proficient precursors for synthesizing novel compounds of biological importance. Metal chelates of biologically active Schiff bases have been found more efficacious than free ligands. Metal complexes of transition metal ions can exhibit amazing pharmacological activities like antimicrobial, antiproliferative, antidiabetic, anti-inflammatory and anticancer while such potential is not noticed when the ligand or inorganic metallic salts are used individually [12–15]. Most appropriate metals for aforementioned purpose are transition metals because transition metals can exhibit different geometries and coordination numbers along with variable oxidation states as compared to other main group metals. Nickel is found in active sites of many enzymes like hydrogenases and CO-dehydrogenases. In its common oxidation state of + 2, numerous nickel complexes have shown their importance in antimicrobial and antiproliferative activities [16]. Zinc metal possesses crucial position in metabolism, immune response, functioning of liver and strengthening of bones being a part of enzymes for example alkaline phosphate enzyme, superoxide dismutase, alcohol dehydrogenase and protein kinase-C. Cu(II) and Zn(II) metal composites have been the subject of vast research work due to their excellent fluorescent and antimicrobial properties [17–25]. Cobalt, copper, zinc and nickel metals are well-recognized elements in our biological system. Also the antimicrobial potential of many drugs can be boosted after chelation with transition metals. So it becomes essential to know more about the bonding of ligands with metals and their structural properties to develop operative antimicrobial metal complexes.

The present research comprises of the design and synthesis of a fresh series of transition metal complexes of azomethine being condensation product of anthracene-10-carbaldehyde with 4-amino-3-mercapto-1,2,4-triazin-5(4*H*)-one. Their properties were investigated experimentally by using UV–visible, proton-NMR, IR, fluorescence, ESR spectroscopic techniques and cyclic voltammetry. Additionally, thermal profiles of the metal complexes were examined by thermogravimetric analysis. The bioactivities like antimicrobial and antifungal of all synthesized compounds have been reported here.

Experimental section

Materials and methods

Chemicals

All chemicals were of reagent grade. Acetate salts of Co(II), Ni(II), Cu(II), Zn(II) and anthracene-10-carbaldehyde were obtained from Sigma-Aldrich and used as supplied. Solvents such as dimethylformamide (DMF), dimethyl sulphoxide (DMSO), ethanol, acetic acid, diethylether and methanol were of analytical grade and used as received without further purification.

Instrumentation

Infrared (IR) spectra of the pure compounds were acquired on a MB3000 ABB spectrophotometer in 4000–30 cm^{-1} range using KBr pellets. ^{1}H-NMR spectra of the synthesized free ligand and zinc complexes were obtained in deuterated DMSO using tetramethylsilane (TMS) as internal standard on a JEOL-400 NMR spectrometer. Thermo Scientific flash 2000 CHN Elemental Analyzer was adopted for C, H and N analyses of compounds at central instrumentation laboratory (CIL), Punjab University, Chandigarh. Estimation of nickel, zinc and copper metal ions was carried out by gravimetric methods, and cobalt was estimated by titration with 0.01 M EDTA [26]. Mass spectra were recorded on Waters Xevo G2-SX QTOF spectrophotometer. Electronic data of ligand and its complexes were obtained on T-90 (PG instruments Ltd.) UV–visible spectrophotometer in 900–190 nm range. EPR spectral information of copper samples were obtained using Varian E112 X-Band Spectrophotometer employing at 9.097 GHz frequency and field was calibrated with 2,2-Diphenyl-1-picrylhydrazyl (DPPH) at the SAIF, IIT Bombay. Magnetic properties of the samples were recorded on a vibrating sample magnetometer of model PAR-155, in which $Hg[Co(CNS)_4]$ was used as calibrant. Thin layer chromatographic plates were used to check the purity of ligand and metal chelates. Molar conductance of the complexes in DMF solution was measured using Systronics conductivity bridge. The Perfit electrical melting point apparatus was employed for recording melting points. The fluorescence spectra of all samples were monitored on SHIMADZU RF-5301 PC spectrofluorometer in dimethylformamide solution. Thermogravimetric analysis of metal complexes was achieved under nitrogen atmosphere at a heating rate of 10 °C per minute at Central Instrumentation Facility (CIF), LPU, Phagwara. Ivium Stat Electrochemical

Analyzer was employed to perform electrochemical study of compounds using tertbutyl ammonium perchlorate as a supporting salt.

Biological activity investigation

Agar well diffusion method was applied for antibacterial examination as described in our former research paper [4]. The antibacterial activities of synthesized samples have been checked with regard to two Gram-positive bacteria (*Staphylococcus aureus* MTCC-96, *Bacillus subtilis* MTCC-121) and two Gram-negative bacteria (*Escherichia coli* MTCC-1652, *Candida albicans* MTCC-183) on nutrient agar medium. *S. aureus* is a member of microbiota of the body and possesses thick peptidoglycan layer. It causes joint infections, pneumonia, skin infections like boils and cellulitis. *B. subtilis* is non-pathogenic, Gram-positive bacteria. Although, it is one of the most commonly used bacteria for the production of enzymes still B. subtilis causes endocarditis, pneumonia and septicemia. However, these infections were noted in patients having very low immunity. *E. coli* are non-sporing with thin cell walls and lower intestine of warm-blooded animals is their primary habitat. These can cause various diseases like intestinal infections for e.g. UTIs, sepsis, meningitis, etc. *C. albicans* lies in category of pathogenic yeast, found in mouth and gastrointestinal tract of adults. It is one of the frequently isolated organisms involved in bloodstream infections. *A. flavus* is the most widely distributed fungi accountable for aflatoxin contamination of foodstuffs. It is also known for the production cancer-causing groups of mycotoxins. *Aspergillus niger* is a food spoilage fungus. It is one of the major causes of 'black mould' that is found on the surfaces of certain foods.

The antifungal activities were checked against two fungal types (*Aspergillus niger* MTCC-872 and *Aspergillus flavus* MTCC-873) by poisoned food technique. Solutions of compounds were prepared in dimethyl sulphoxide (DMSO). Agar medium was shifted to petri plates and plates were swabbed with 100 µL inocula of test microorganisms and kept for 15–20 min for adsorption. Using a sterile cork borer of 8 mm diameter, wells were bored in medium of agar plates, already seeded with the test microorganisms. 200 µL of every sample was poured in each well. The agar plates were preserved at 4 °C for minimum 30 min to let the dispersal of the sample to agar channel. The plates were then incubated at 37 °C for bacteria and 30 °C for fungi, respectively. The diameters of inhibition zones were specified after 24 h and 7 days for bacteria and fungi, respectively, taking the consideration of the control values (DMSO). Diameters of fungal colonies were determined as mycelial inhibition percentage.

$$\text{Inhibition percentage of mycelial growth} = \left(d_c - d_t\right)/d_c \times 100$$

Where d_c is mean diameter of fungal colony in DMSO control and d_t is mean diameter of fungal colony in experimental samples. Each experiment was performed in triplicates. Ciprofloxacin and Fluconazole were utilized as standard drugs with respect to bacteria and fungi separately. The minimal concentration of all samples which hindered the growth of bacteria was also checked and reported as minimum inhibitory concentration (MIC).

Syntheses

Synthesis of 4-(anthracen-10-ylmethyleneamino)-3-mercapto-1,2,4-triazin-5(4*H*)-one (Scheme 1)

4-amino-3-mercapto-1,2,4-triazin-5(4*H*)-one (AMTO) was prepared using reported literature [27]. Equimolar ethanolic solutions of AMTO (1.58 g, 11 mmol) and anthracene-10-carbaldehyde (2.27 g, 11 mmol) containing few drops of acetic acid were mixed and maintained under reflux for 90 min. Crystalline yellow solid was recovered after cooling the reaction mixture. The product was separated by filtration, washed with cold ethanol and diethylether and recrystallized to obtain pure ligand corresponding to 81% yield. Scheme given below illustrates the formation of ligand.

Synthesis of 1:1 transition metal complexes

Hot stirred ethanolic solutions of the ligand (0.298 g, 0.9 mmol, 20 mL) and acetates of cobalt (0.224 g, 0.9 mmol), nickel (0.224 g, 0.9 mmol), copper (0.180 g, 0.9 mmol) and zinc (0.198 g, 0.9 mmol) were mixed gradually corresponding to 1:1 (M:L) molar ratio. The mixtures were maintained under reflux with stirring nearly for 2 h. Resulting coloured precipitates were filtered out and washed with small portions of ethanol, diethyl ether and then kept in a desiccator in the presence of anhydrous $CaCl_2$.

Synthesis of 1:2 transition metal complexes

For preparation of 1:2 (M:L) metal complexes, ethanolic solutions of above stated amounts of metal acetates of cobalt, nickel, copper and zinc were reacted with heated ethanolic solutions of ligand (0.596 g, 1.8 mmol). Then reaction mixtures had been refluxed for about 2 h. Coloured solid products were filtered out, washed with small portions of ethanol and diethyl ether. Final products were placed in a desiccator over anhydrous $CaCl_2$.

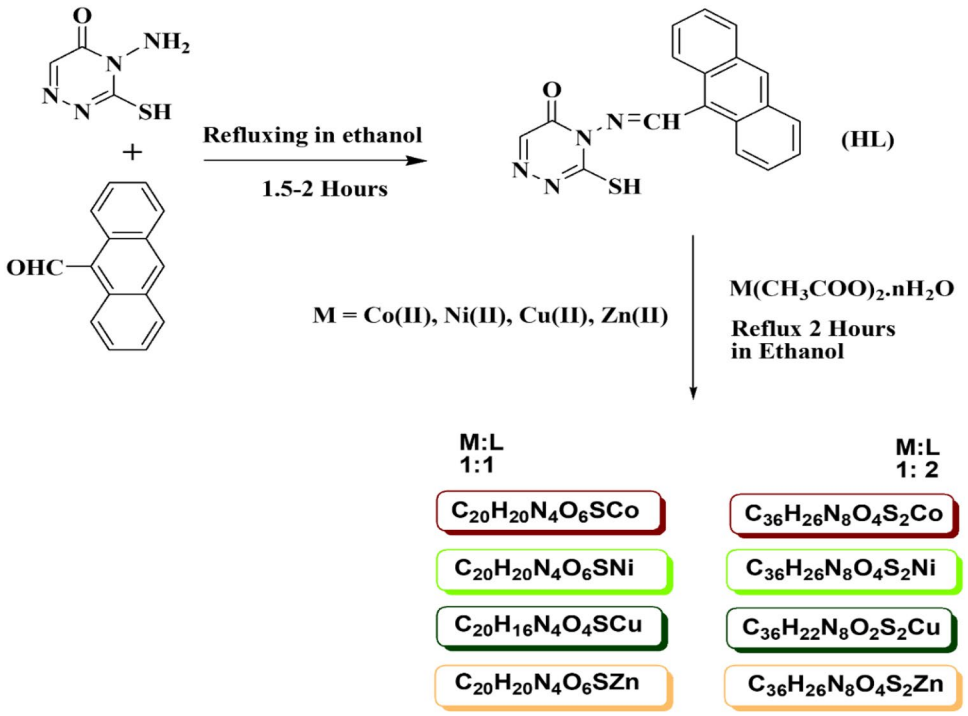

Scheme 1 Synthetic route of 4-(Anthracen-10-ylmethyleneamino)-3-mercapto-1,2,4-triazin-5(4*H*)-one and its metal chelates

Results and discussion

The ligand and metal complexes are coloured, air-stable, non-water absorbing and get decomposed at higher temperature. The metal complexes are soluble in DMSO, DMF and acetone and not soluble in other conventional organic solvents. The molar conductance values of metal complexes in DMF (10^{-4} M) are in the range of 10.24–21.40 Ω^{-1} cm^2 mol^{-1}, such low conductance values suggest non-electrolytic behaviour of metal complexes. Some physical and elemental analysis data are depicted in Table 1.

IR spectral studies

Bonding of metal ions to the ligand may be determined by assessing IR spectra of the metal complexes and ligand. So, the ligand and its metal complexes have been characterized with IR spectral studies (Table 2). The further deductions can be drawn: The infrared spectrum of ligand exhibits a strong band at 1636 cm^{-1} due to υ (C=O) of triazine part. No significant change in the carbonyl band position in the IR spectra of the metal complexes, designates that the carbonyl group in these complexes is not involved in coordination to the metal ions [28]. A medium intensity

Table 1 Molar conductivity, melting point, colour and elemental analysis of Schiff base (HL) and its metal complexes

Compounds	Colour	Melting point (°C)	Molar conductivity (Ω^{-1} cm^2 mol^{-1})	Elemental analysis calculated (found) %			
				C	H	N	M
$C_{18}H_{12}N_4OS$	Yellow	240	18.90	65.04 (64.44)	3.64 (3.27)	16.86 (16.21)	–
$C_{20}H_{20}N_4O_6SCo$	Dark brown	314^d	11.65	47.72 (46.64)	4.00 (3.45)	11.13 (11.08)	11.71 (11.24)
$C_{36}H_{26}N_8O_4S_2Co$	Dark brown	322^d	10.24	57.07 (57.18)	3.46 (3.33)	14.79 (13.95)	7.78 (6.98)
$C_{20}H_{20}N_4O_6SNi$	Yellowish green	320^d	17.85	47.74 (46.39)	4.01 (3.56)	11.14 (10.69)	11.67 (10.86)
$C_{36}H_{26}N_8O_4S_2Ni$	Yellowish green	324^d	18.21	57.08 (57.11)	3.46 (2.99)	14.79 (13.68)	7.75 (6.82)
$C_{20}H_{16}N_4O_4SCu$	Olive green	332^d	20.13	50.90 (50.10)	3.42 (3.25)	11.87 (11.56)	13.46 (13.23)
$C_{36}H_{22}N_8O_2S_2Cu$	Olive green	328^d	21.40	59.53 (59.01)	3.05 (2.92)	15.43 (15.17)	8.75 (8.41)
$C_{20}H_{20}N_4O_6SZn$	Pastel orange	318^d	16.13	47.11 (46.32)	3.95 (3.31)	10.99 (10.12)	12.83 (12.26)
$C_{36}H_{26}N_8O_4S_2Zn$	Pastel orange	320^d	15.90	56.58 (56.23)	3.43 (3.19)	14.66 (13.72)	8.56 (7.29)

d = decomposed

Table 2 IR spectral frequencies (cm^{-1}) of studied compounds

Compounds	ν(N=CH)	ν(S–H)	ν(OAc)	ν(H_2O/OH)	ν(M–N)	ν(M–S)
$C_{18}H_{12}N_4OS$	1589	2700	–	–	–	–
$C_{20}H_{20}N_4O_6SCo$	1574	–	1744	3248	469	342
$C_{36}H_{26}N_8O_4S_2Co$	1574	–	–	3271	458	338
$C_{20}H_{20}N_4O_6SNi$	1582	–	1744	3294	482	342
$C_{36}H_{26}N_8O_4S_2Ni$	1582	–	–	3225	470	342
$C_{20}H_{16}N_4O_4SCu$	1561	–	1740	3310	482	338
$C_{36}H_{22}N_8O_2S_2Cu$	1566	–	–	–	484	340
$C_{20}H_{20}N_4O_6SZn$	1582	–	1744	3209	468	340
$C_{36}H_{26}N_8O_4S_2Zn$	1582	–	–	3290	469	338

band observed in IR spectrum of ligand at 1589 cm^{-1} is assigned to ν(CH=N) azomethine group which gets shifted to lower wavenumber, 1561–1582 cm^{-1} in the IR spectra of metal complexes indicating the coordination of azomethine nitrogen to metal ions [29]. The double bond character of the azomethine group decreases due to the attachment of nitrogen atoms to the metal ions and hence corresponding band gets shifted. These results are consistent with the outcomes obtained from similar structured compounds documented by researchers [30]. New absorption bands in low frequency regions 458–484 cm^{-1} and 338–342 cm^{-1} are observed due to ν(M–N) and ν(M-S), respectively [31]. A weak band at 2700 cm^{-1} is observed due to ν(SH) in the spectrum of Schiff base which gets disappeared on complexation, indicating deprotonation of thiol group and coordination through sulphur [32]. In the IR spectra of 1:1 metal complexes, characteristic band in region 1740–1744 cm^{-1} was attributed to ν(OAc). Asymmetric ν_{as}(OAc) and symmetric ν_s(OAc) stretches in metal complexes occur at about 1591–1594 cm^{-1} and 1373–1388 cm^{-1}, respectively, with wavenumber separation of $\Delta\nu = 203–221$ cm^{-1} indicating monodentate nature of acetate group [33]. The broad bands were emerged in the region 3209–3310 cm^{-1} due to ν(OH/H_2O) vibrations of coordinated water molecules in IR spectra of all the complexes except in 1:2 Cu(II) metal complex [34]. Further existence of water molecules in coordination spheres of compounds was endorsed by thermogravimetric studies.

^{1}H-NMR spectroscopy

^{1}H-NMR spectra of HL and its zinc metal chelates were recorded in DMSO-d_6 (Figs. S2-S4 in supporting information) and data are presented in Table 3. A singlet was observed at δ 8.92 ppm due to azomethine proton (–CH=N) in the ligand which got shifted to δ 8.96 ppm and δ 8.95 ppm in 1:1 and 1:2 Zn complexes, respectively, clearly indicating coordination of azomethine nitrogen to zinc ions [35]. Another singlet at δ 14.15 ppm corresponding to thiol proton (–SH) in ligand's spectrum got disappeared in spectra of Zn(II) complexes propounding deprotonation of thiol group and further coordination of sulphur to zinc metal ions [36]. In the ^{1}H-NMR spectrum of ligand (supporting information Fig. S1), aromatic protons H_a and H_d exhibit doublet at 8.91 and 8.24 ppm, respectively, with 8.4 Hz coupling constant. Two multiplets are observed in the range 7.73–7.69 ppm and 7.66–7.63 ppm corresponded to H_b and H_c protons of anthracene moiety. A singlet at 8.06 ppm in ligand's spectrum, is due to aromatic proton of triazine ring. Signals at 4.32 ppm and 4.22 ppm are due to coordinated water molecules in 1:1 and 1:2 Zn complexes, respectively. The signal due to acetate group is only observed in 1:1 Zn compound at 1.31 ppm. Obtained ^{1}H-NMR data of ligand and zinc metal complexes were also compared to that of similar structured compounds. The results reveal that signal due to azomethine proton got shifted in complexes and signals due to phenol/thiol hydrogen are disappeared

Table 3 ^{1}H-NMR data of HL and Zn(II) complexes

Compounds	Chemical shifts (ppm)
$C_{18}H_{12}N_4OS$	8.92 (s, 1H, –N=CH), 14.15 (s, 1H, –SH), 8.91 (d, 2H, Ar–H, J = 8.4 Hz), 8.24(d, 2H, Ar–H, J = 8.4 Hz), 9.89 (s, 1H, Ar–H), 7.66–7.63 (m, 2H, Ar–H), 7.73–7.69 (m, 2H, Ar–H), 8.06 (s, 1H, triazine)
$C_{20}H_{20}N_4O_6SZn$	8.96 (s, 1H, –N=CH–), 8.94 (s, 1H, Ar–H), 8.89 (s, 1H, Ar–H), 8.21 (d, 2H, Ar–H, J = 8 Hz), 9.87 (s, 1H, Ar–H), 7.68–7.56 (m, 4H, Ar–H), 8.13 (s, 1H, triazine), 1.31 (s, 3H, $OCOCH_3$), 4.32 (s, 6H, H_2O)
$C_{36}H_{26}N_8O_4S_2Zn$	8.95 (s, 2H, –N=CH–), 8.91 (d, 4H, Ar–H, J=16 Hz), 8.21 (d, 4H, Ar–H, J = 8.4 Hz), 9.90 (s, 2H, Ar–H), 7.70–7.67 (m, 4H, Ar–H), 7.64–7.61 (m, 4H, Ar–H), 8.13 (s, 2H, triazine), 4.22 (s, 4H, H_2O)

in case of metal complexes which confirm the binding of O^- or S^- to the metal centres [25].

Mass spectral studies

Formulation of ligand and its metal chelates has been determined from elemental analytical data, IR and NMR spectroscopy which is further supported by mass spectrometry. Mass spectra of some samples showed molecular ion peaks at m/Z 332.13, 505.39, 504.52, 726.04, 763.88 correspond to their molecular formulas $C_{18}H_{12}N_4OS$, $C_{20}H_{20}N_4O_6SCo$, $C_{20}H_{20}N_4O_6SNi$, $C_{36}H_{22}N_8O_2S_2Cu$, $C_{36}H_{26}N_8O_4S_2Zn$, respectively. These results support ML type stoichiometry in 1:1 cobalt and nickel metal complexes and ML_2 type stoichiometry in 1:2 copper and zinc metal complexes. The series of peaks other than molecular ion peaks are indicative of various fragments in samples and intensity of each peak suggests its stability among all fragments [37]. A good agreement between suggested molecular formula by elemental analysis and molecular ion peaks by mass spectral data is observed. Mass spectra of compounds are shown in Figs. S5-S9 (Supporting information).

Magnetic moment measurements and electronic spectral studies

The magnetic moment measurements along with electronic spectral data afforded much knowledge concerning the arrangement of the ligand around the metal centres which is represented in Table 4. Absorption spectra of all compounds were noted in solvent DMF with concentration 50 µm at room temperature. Ligand showed two intense maxima in its spectrum at 36,101 cm^{-1} and 28,328 cm^{-1} owing to π–π^* and n–π^* transitions. Bathochromic shifts in these transitions were noted in metal complexes which endorses metal–ligand coordination in chelates.

Cobalt complexes

Both Co(II) complexes showed magnetic moment 4.53–4.62 BM, which is properly inside the anticipated range of octahedral complex, i.e. 4.3–5.2 BM. Co(II) complexes display two absorption bands in region 10,101–10,351 cm^{-1} (ν_1) and 20,920–21,186 cm^{-1} (ν_3) assigned to spin allowed $^4T_{1g} \rightarrow {}^4T_{2g}$(F) and $^4T_{1g} \rightarrow {}^4T_{1g}$(P) transitions, respectively, which signify distinctive bands shown by octahedral Co(II) complexes of high spin [38]. ν_2 value is not observed in electronic spectra but it has been calculated by using relation $\nu_2 = \nu_1 + 10Dq$. Ligand field factors like crystal field stabilizing energy, Racah parameter (B), nephelauxetic ratio (β) and β% have also been computed for these complexes with Band-fitting equation [39]. The crystal field stabilizing energy (Dq) values were located at 1133.6 and 1160 cm^{-1}. These values properly lie in the range shown by octahedral compounds. The interionic repulsion parameter (Racah parameter), i.e. B, is found to be 776.3–803.5 cm^{-1} implying a generous overlapping of ligand and metal orbitals. The value of β (nephelauxetic ratio) below unity advises partial covalency in the metal ligand bond in these complexes [40].

Nickel complexes

Nickel complexes, with magnetic moment in the range 3.29–3.47 BM exhibit octahedral atmosphere around the central metal. Nickel(II) complexes mostly show three absorption bands for spin allowed d–d transitions corresponding to $^3A_{2g} \rightarrow {}^3T_{2g}$ (F) (ν_1), $^3A_{2g} \rightarrow {}^3T_{1g}$ (F) (ν_2) and $^3A_{2g} \rightarrow {}^3T_{1g}$ (P) (ν_3) transitions which are compatible with octahedral environment around nickel centres. Here, both 1: 1 and 1: 2 Ni(II) complexes of HL show above-mentioned three transitions in region 10,362–10,373 cm^{-1} (ν_1), 17,035–17,094 cm^{-1} (ν_2) and 24,038–24,154 cm^{-1} (ν_3) signifying distorted octahedral geometry for the complexes [41]. The ratio ν_2/ν_1 (1.64–1.65) supported the octahedral environment around the central metal ion. Other important crystal field parameters (β%, Dq, β, B) were also computed for these compounds which reveal covalent nature of nickel-ligand bonds [42].

Table 4 UV–Visible, ligand field parameters and magnetic moment data of Co(II), Ni(II) and Cu(II) metal complexes

Compounds	Transitions (cm^{-1})			Dq (cm^{-1})	υ_2/υ_1	B (cm^{-1})	β	β%	Magnetic Moment (µ) B.M
	υ_1	υ_2	υ_3						
$C_{20}H_{20}N_4O_6SCo$	10,351	21,951	20,746	1160.0	776.3	2.12	0.80	20	4.53
$C_{36}H_{26}N_8O_4S_2Co$	10,101	21,435	20,920	1133.4	803.5	2.12	0.86	14	4.62
$C_{20}H_{20}N_4O_6SNi$	10,362	17,035	24,154	1036.2	673.5	1.64	0.65	35	3.29
$C_{36}H_{26}N_8O_4S_2Ni$	10,373	17,094	24,038	1037.3	667.5	1.65	0.64	36	3.47
$C_{20}H_{16}N_4O_4SCu$	17,605	–	–	–	–	–			2.02
$C_{36}H_{22}N_8O_2S_2Cu$	17,793	–	–	–	–	–			1.91

Copper complexes

Cu(II) complexes have 1.91– 2.02 BM magnetic moment values which fall in the normal range (1.7–2.2 BM) for square planar geometry. The electronic spectra of Cu(II) complexes showed broad absorption band at about 17,605–17,793 cm^{-1} which is attributed to overlapped transitions, i.e. $^2B_{1g} \rightarrow {}^2A_{1g}$ and $^2B_{1g} \rightarrow {}^2B_{2g}$ [43]. It is a representative band of square planar geometry around the Cu(II) centre [4, 44].

Electron spin resonance study

To know more about type of bonding between metal and Schiff base, ESR analysis of copper complexes was performed. ESR spectra of copper metal complexes were monitored in magnetic field strength of 0.3 T at liquid nitrogen temperature, on X-band at 9.097 GHz using TCNE as marker. ESR studies also give information about location of unpaired electron in different orbitals. The values of g-tensor are observed in order: $g_{\parallel}(2.26) > g_{\perp}(2.10) > 2.0023$ for $C_{20}H_{16}N_4O_4SCu$ and $g_{\parallel}(2.27) > g_{\perp}(2.07) > 2.0023$ for $C_{36}H_{22}N_8O_2S_2Cu$ complex. Experimental data indicate that single electron rests in $d_{x^2-y^2}$ orbital primarily and $^2B_{1g}$ can be designated as ground state. This observation also commended square planar geometry of both complexes [31]. Exchange interaction parameter (G) was computed from equation $G = \frac{g_{\parallel}-2.0023}{g_{\perp}-2.0023}$. Exchange interaction is negligible if $G > 4$ and extensive exchange interaction is found in the metal complexes if it is smaller than 4. The G values are found less than 4, confirming exchange interactions amid Cu(II) centres [45]. Deviation of g_{av} from 2.0023 (g_e) indicates covalent character of metal–ligand bonds in both copper complexes. The $g_{\parallel} < 2.3$ also confirm covalent M-L linkages. The empirical factor, $f = g_{\parallel}/A_{\parallel}$, is an indicator of deformation and varies from 105–135 cm^{-1} for minor to major distortion in square planar geometries moreover values lower than 135 cm^{-1} are observed for square planar structures. The f values for 1:1 and 1:2 copper complexes are 82.48 and 93.03, respectively, supporting square-planar geometry. ESR spectrum of $C_{20}H_{16}N_4O_4SCu$ is displayed in Fig. 1. Molecular orbital coefficients, α^2

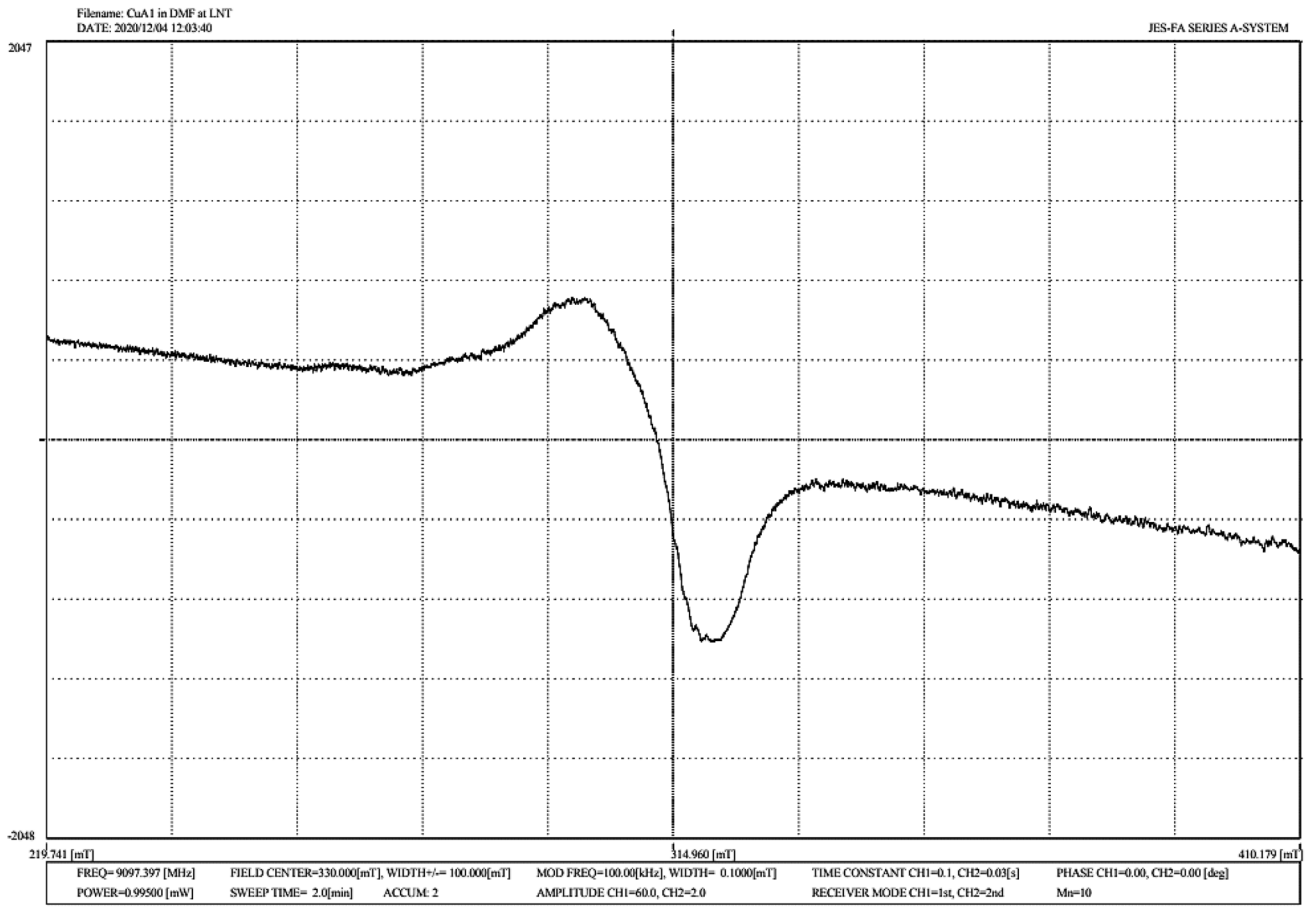

Fig. 1 ESR spectrum of $C_{20}H_{16}N_4O_4SCu$ complex

(covalent in-plane sigma bonding), β^2 (covalent in-plane pi-bonding) and γ^2 (out of plane pi-bonding), were calculated to better define the nature of M-L bonds, using following equations.

$$\alpha^2 = \left(\frac{A_\parallel}{0.036}\right) + \left(g_\parallel - 2.0023\right) + \frac{3\left(g_\perp - 2.0023\right)}{7} + 0.04$$

$$\beta^2 = \left(g_\parallel - 2.0023\right)E/ - 8\lambda\alpha^2$$

$$\gamma^2 = \left(g_\perp - 2.0023\right)E/ - 2\lambda\alpha^2$$

The 0.5 value of α^2 directs ample covalent bonding, while 1.0 value advises ionic bonding. Since α^2 values for invested copper complexes lie near ~ 1.0 which is anticipated for partial ionic nature of the bonds [46]. Observed β^2 values (0.62 and 0.70) are less than unity and also less than α^2 values which indicate the presence of more in-plane π–bonding than in-plane σ-bonding in metal complexes. Values of $A_\parallel$ for copper complexes are found greater than 140×10^{-4} cm^{-1}, i.e. 274×10^{-4} and 244×10^{-4} cm^{-1}, which further supports square planar arrangement around copper centres in both complexes [47]. According to Hathaway and Billing, for pure sigma bonding, the relation between orbital reduction factors is $K_\parallel > K_\perp \approx 0.77$, $K_\parallel < K_\perp$ for in-plane π–bonding while $K_\parallel > K_\perp$ for out of plane π–bonding. The equations are:

$$K_\parallel = \left(g_\parallel - 2.0023\right)E/8\lambda$$

$$K_\perp = \left(g_\perp - 2.0023\right)E/2\lambda$$

Examined $K_\parallel$ (0.68, 0.71) and $K_\perp$ (1.03, 0.73) values for both complexes imply larger impact of in-plane pi-bonding than out of plane pi-bonding in M-L linkages. Also, greater $K_\perp$ values than $K_\parallel$ indicate the presence of significant in-plane π–bonding which supports the results obtained from molecular orbital parameters.

Redox properties

Cyclic voltammograms of copper chelates were monitored in DMF containing 0.1 M of tetrabutylammonium perchlorate electrolyte with a scan rate of 0.01 Vs^{-1} in a potential range − 1.5 V to + 1.0 V to enquire their redox properties. In recorded voltammogram of 1:1 Cu complex, two peaks are observed at $E_{pc} = 0.34$ V and $E_{pc'} = -0.45$ V assigned for the reactions Cu(II) to Cu(I) and Cu(I) to Cu(0) independently on the reduction side and likewise two peaks associated with Cu(0) to Cu(I) and Cu(I) to Cu(II) are observed at $E_{pa} = -0.18$ V and $E_{pa'} = 0.60$ V on the oxidation side. These couples are quasi-reversible with high values of ΔE_p, i.e. 260 mV and 270 mV. 1:2 Cu complex exhibits two redox couples; one is observed at $E_{pc} = 0.235$ V on reduction side and at $E_{pa} = 0.36$ V on oxidation side for Cu(II)/Cu(I) and another redox couple Cu(I)/Cu(0) is observed at $E_{pc'} = -0.44$ V on reduction side and at $E_{pa'} = -0.245$ V on oxidation side. Ratio of anodic to cathodic peak currents for redox couples lie in range 0.26–0.72 and 0.21–1.83 for 1:1 Cu complex and 1:2 Cu complex, respectively, which suggest non-equivalent current intensity and are consistent with quasi-reversible processes. $\Delta E_p = 125$ mV and 195 mV values of redox couples of 1:2 Cu complex suggest quasi-reversible processes [48, 49]. When these cyclic voltammograms were compared with that of ligand, it was found that there is no oxidation and reduction peaks in CV of ligand. Cyclic voltammogram of copper complexes are exposed in Fig. 2.

Thermogravimetric analysis

Some of prepared metal complexes were examined for their thermal properties. Thermogravimetric curves of $C_{36}H_{26}N_8O_4S_2Co$, $C_{20}H_{20}N_4O_6SNi$, $C_{20}H_{16}N_4O_4SCu$ and $C_{36}H_{26}N_8O_4S_2Zn$ complexes are shown in Fig. 3. These

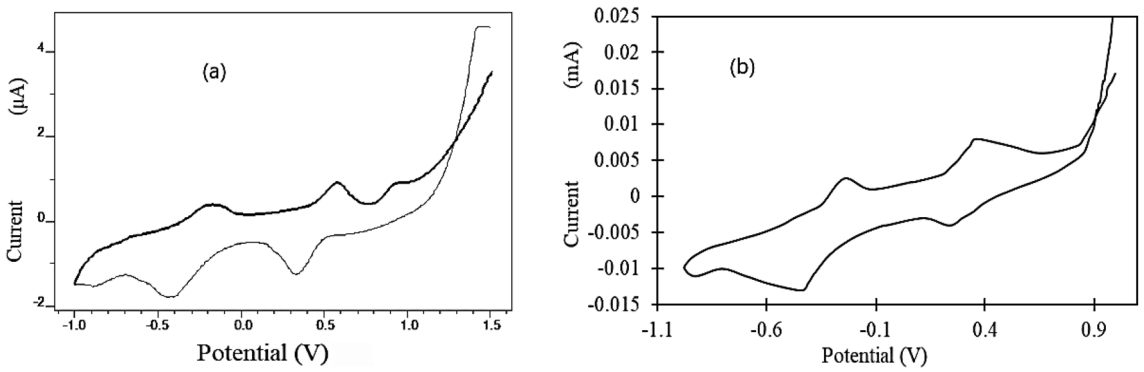

Fig. 2 Cyclic voltammograms of **a** 1:1 Cu complex **b** 1:2 Cu complex

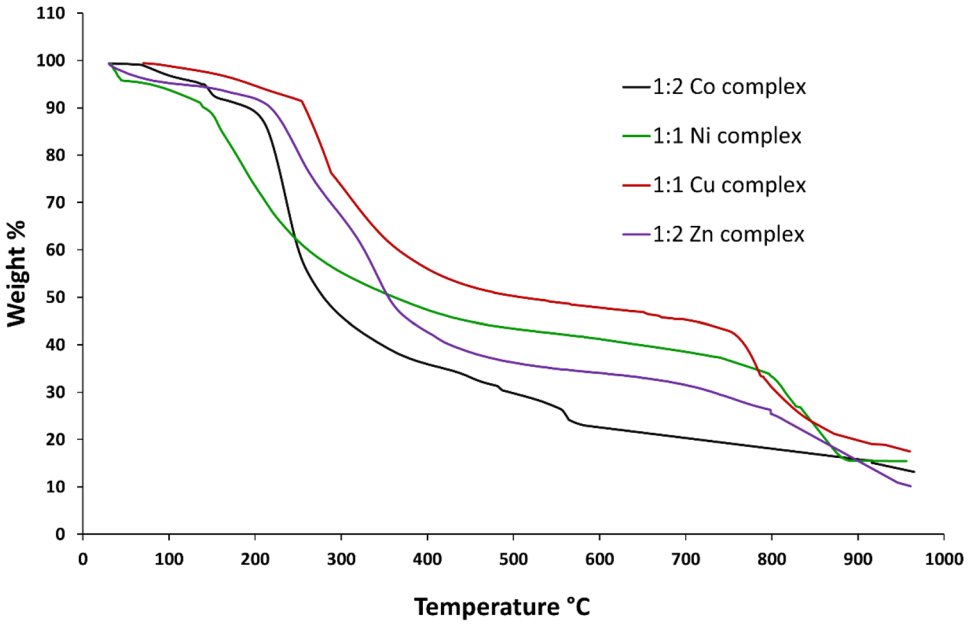

Fig. 3 Thermogravimetric curves of metal complexes

complexes followed a similar pattern of decomposition. The degradation temperatures with decomposed moieties and mass loss percentages of these metal complexes along with their residues are illustrated in Table 5.

The complex $C_{36}H_{26}N_8O_4S_2Co$ decomposes in three different stages. First decomposition stage in temperature range 80–140 °C may be ascribed to loss of coordinated water molecules with a weight loss of 4.79% (calculated 4.75%). The second step of decomposition in temperature range 141–575 °C might attribute to loss of organic moiety with found weight loss 53.39% (calculated 53.84%) and the final stage of decomposition between temperature 576 °C and 920 ˚C corresponded to loss of triazine moiety with weight loss 28.66% (calculated 29.30%). After these degradation steps, final weight of residue corresponded to CoS [50, 51].

The compound $C_{20}H_{20}N_4O_6SNi$ degrades in three steps. The first step owes in mass loss of 9.93% (calculated 10.73%) in temperature range 80–144 ˚C equivalent to weight loss of three H_2O molecules. Then, organic part of molecule gets decomposed with mass loss of 48.75% (calculated 49.48%) between temperature range (145–600 ˚C). Last step involves a weight loss of 25.78% (calculated 24.84%) in the temperature range 601–956 ˚C due to decay of triazine moiety. $C_{20}H_{16}N_4O_4SCu$ degrades in three stages. The first one seems to be sufficient to weight loss of coordinated water molecule and acetate group with found weight loss of 15.46% (calculated 16.31%) between 100 and 270 ˚C. In second stage, decomposition of organic moiety takes place from 271 to 720 ˚C with weight loss of 40.02% (calculated 40.25%). In the third step decomposition occurs between

Table 5 Different decomposition stages, moieties, calculated and found weight losses of selected metal complexes of HL

Compounds	Temp (˚C)	% Weight loss, found (calculated)	Decomposed moieties	Metallic residue (%) found (calculated)
$C_{36}H_{26}N_8O_4S_2Co$	80–140 141–575 576–920	4.79 (4.75) 53.39 (53.84) 28.66 (29.30)	(i) Water molecules, H_4O_2 (ii) Organic Moiety, $C_{30}H_{20}N_2$ (iii) Triazine Moiety, $C_6N_6H_2SO_2$	CoS 13.16 (12.01)
$C_{20}H_{20}N_4O_6SNi$	80–144 145–600 601–956	9.93 (10.73) 48.75 (49.48) 25.78 (24.84)	(i) Water molecules, H_6O_3 (ii) Organic Moiety and acetate group, $C_{17}H_{13}O_2$ (iii) Triazine Moiety, C_3N_4HS	NiO 15.54 (14.84)
$C_{20}H_{16}N_4O_4SCu$	100–270 271–720 721–960	15.46 (16.31) 40.02 (40.25) 27.04 (26.48)	(i) Water molecules and acetate group, $C_2H_5O_3$ (ii) Organic Moiety, $C_{15}H_{10}$ (iii) Triazine Moiety, C_3N_4HS	CuO 17.48 (16.85)
$C_{36}H_{26}N_8O_4S_2Zn$	80–130 131–510 511–960	4.94 (4.71) 59.15 (58.10) 26.51 (26.43)	(i) Water molecules, H_4O_2 (ii) Organic Moiety, $C_{30}H_{20}S_2$ (iii) Triazine Moiety, $C_6N_8H_2O$	ZnO 9.40 (10.65)

temperature 721 °C and 960 ˚C corresponded to loss of triazine moiety with a weight loss 27.04% (calculated 26.48%). $C_{36}H_{26}N_8O_4S_2Zn$ also shows three decomposition stages. In first stage, weight loss of 4.94% (calculated 4.71%) corresponds to loss of two coordinated water molecules in temperature range 80–130 ˚C. Second stage eliminates organic part of complex between 131 and 510 ˚C temperature with weight loss of 59.15% (calculated 58.10%) and in last step of decomposition triazine moieties are liberated with a weight loss of 26.51% (calculated 26.43%) in temperature range 511–960 ˚C.

Kinetic studies

Well-observed decomposition stages were selected to measure kinetic parameters of metal chelates. Activation energies of decomposition stages have been calculated by applying Coats and Redfern method [52]. Coats and Redfern equation is written as:

$$ln\left[\frac{g(\alpha)}{T^2}\right] = ln\left[\frac{AR}{E\beta}\right] - \frac{E}{RT}$$

where T is temperature; A is pre-exponential factor (min^{-1}); R is universal gas constant (8.314 J/K/mol), E is energy of activation (kJ/mol); β is heating rate (°C min^{-1}); α is degree of conversion; g(α) is decomposition mechanism and $g(\alpha) = \frac{1}{1-\alpha} - 1$ (in case of second order reaction). Activation energy was obtained from the slope of the plot between $ln\left[\frac{g(\alpha)}{T^2}\right]$ and 1000/T. Apparent activation energies for different decomposition stages by applying Coats and Redfern method and analogous regression coefficient values (R^2) are presented in Table 6 and graphs are displayed in Fig. 4. Activation energy values (E_2) of major decomposition step followed the sequence Zn(II) > Cu(II) > Co(II) > Ni(II) complexes and suggested similar thermal stability order of these metal complexes [36].

Table 6 Activation energy values (kJ/mol) for degradation phases of metal chelates using Coats Redfern Method

Metal Complex	Degradation Temperature (˚C)	Activation Energy (kJ mol^{-1})	Regression Coefficient (R^2)
$C_{36}H_{26}N_8O_4S_2Co$	141–575	20.43	0.953
	576–920	219.78	0.916
$C_{20}H_{20}N_4O_6SNi$	145–600	19.98	0.953
	601–956	17.46	0.992
$C_{20}H_{16}N_4O_4SCu$	271–720	21.71	0.944
	721–960	183.49	0.925
$C_{36}H_{26}N_8O_4S_2Zn$	131–510	31.06	0.988
	511–960	13.56	0.948

Fluorescence spectroscopic studies

Metal complexes fluorescence studies are very important because of their applications such as in photochemistry, luminescent displays and as chemical sensors [11]. The photoluminescent properties of Schiff base and all metal chelates were investigated in DMF solvent at room temperature. The emission spectra were noted in 380–800 nm span of wavelength. The comparable fluorescence spectra of 1:1 and 1:2 metal complexes with Schiff base are presented in Fig. 5. Upon irradiation of UV-light, with excitation wavelength 370 nm, Schiff base exhibited weak fluorescence with respect to all metal complexes which are comparatively highly fluorescent active. Schiff base exhibits fluorescent emission bands 445 nm along with two shoulders at 418 nm and 474 nm which may be attributed to $\pi - \pi^*$ intraligand transitions [53, 54]. The shapes of emission spectra of metal compounds closely resemble to that of their parent Schiff base. So, fluorescence may be assigned due to intraligand transitions or ligand to metal charge transfer processes. This type of fluorescence is called CHEF (Chelation enhancement of fluorescence). Emission intensity of all metal complexes is higher than that of ligand. The fluorescence quenching in case of ligand may be probably due to incident of PET (photoinduced electron transfer) action which is prevented after complexation. The enhancement in emission intensity is suggested because of complexation of ligand and metal ion centres. Rigidity of the ligand is increased after complexation which further causes to minimize the energy loss [19, 55]. These results indicate that the newly synthesized ligand might be appropriate to sense cobalt, nickel, copper and zinc ions. Both cobalt complexes show high intensity fluorescence bands at 449 nm. Although Ni(II) and Zn(II) complexes show maximum emission bands at 447 nm but Zn(II) complexes display more fluorescence intensity than Ni(II) complexes. 1:1 and 1:2 copper chelates flourish intense emission bands at 475 nm. All these complexes also show some shoulder bands along with main higher intensity emission bands. Among all compounds copper chelates are found to possess higher fluorescent properties.

Quantum yield calculations

Quantum yield is stated as the fraction of molecules of a sample that emit photons after excitation by the source. Uncertainties related to apparatus and samples can influence the quantum yield values. So, slit width during the whole experiment was kept constant at 5 mm in order to minimize the uncertainties, also the quinine sulphate

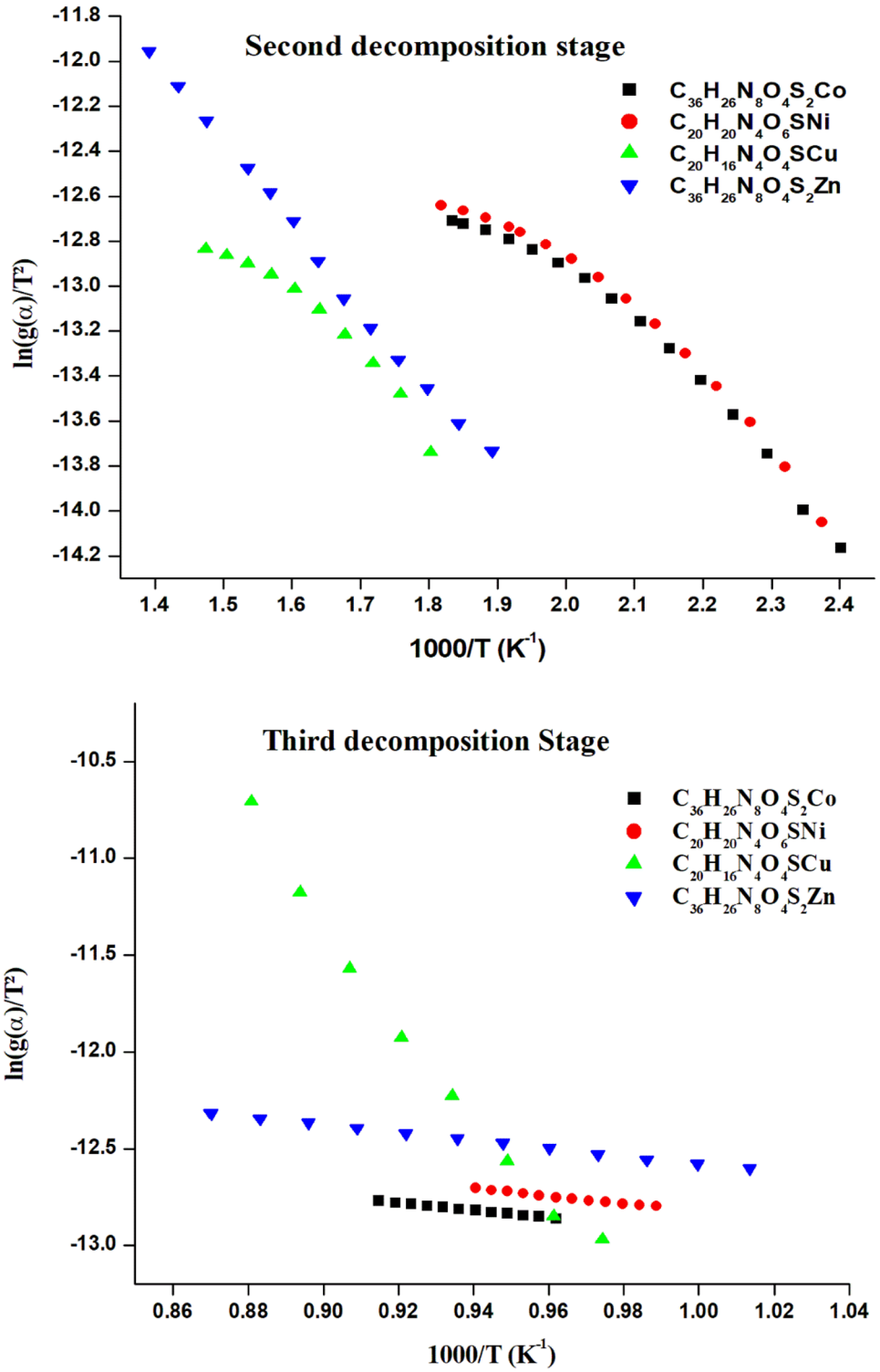

Fig. 4 Coats–Redfern plots for decomposition thermal stages of metal samples

($\varphi_R = 0.54$) was selected as reference solution. Five different concentrations of each sample were prepared in DMF ($\eta_s = 1.4305$) whereas reference was dissolved in 0.1 M H_2SO_4 ($\eta_R = 1.3333$). Fluorescence spectra of all samples were recorded by keeping absorbance values below 0.5. Slopes were determined by plotting the graphs between different concentrations of samples and fluorescence intensity [56]. After knowing the slopes, quantum yields of ligand and metal complexes were calculated by well-known William's method using the following formula:

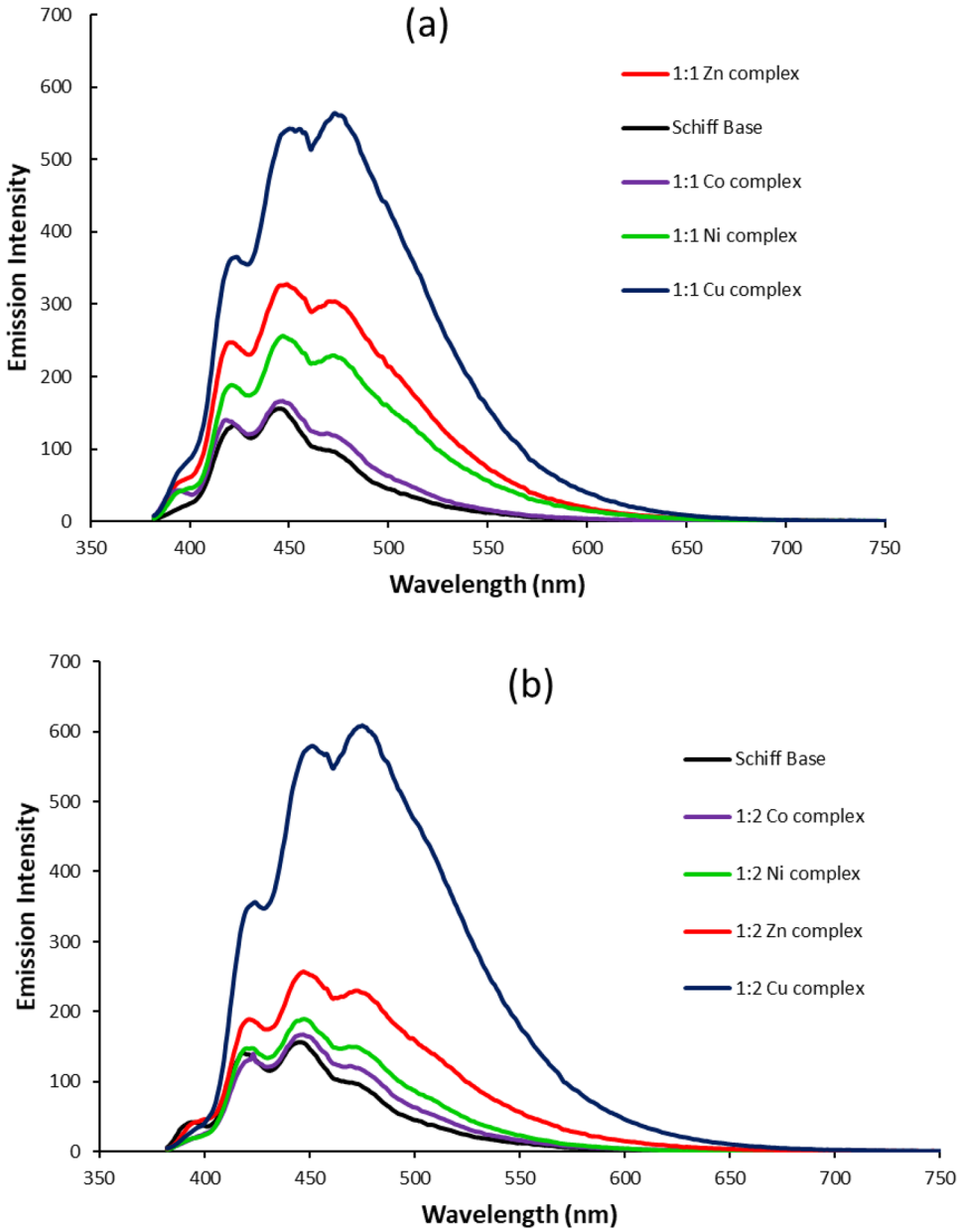

Fig. 5 Fluorescence spectra of Schiff base and its **a** 1:1 metal complexes **b** 1:2 metal complexes

$$\varphi_S = \varphi_R \frac{m_s \eta_S^2}{m_R \eta_R^2}$$

where φ represents quantum yield, *m* values represent slopes of fluorescence intensity versus concentration curves of compounds and η is refractive index of solvent [57]. Subscripts *R* and *S* are taken for reference and sample, respectively. Calculated quantum yields are presented in Table 7. Quantum yield varies from 4.94 to 14.23% and copper complexes exhibit highest quantum yield among all prepared compounds.

Table 7 Quantum yield and CIE parameters of the compounds

Compounds	Slopes	CIE Coordinates		Quantum yield (%)
		(x)	(y)	
$C_{18}H_{12}N_4OS$	61.81	0.16	0.11	4.94
$C_{20}H_{20}N_4O_6SCo$	81.06	0.16	0.12	6.48
$C_{36}H_{26}N_8O_4S_2Co$	77.84	0.16	0.12	6.22
$C_{20}H_{20}N_4O_6SNi$	83.24	0.17	0.19	6.66
$C_{36}H_{26}N_8O_4S_2Ni$	83.78	0.16	0.14	6.70
$C_{20}H_{16}N_4O_4SCu$	177.90	0.17	0.22	14.23
$C_{36}H_{22}N_8O_2S_2Cu$	131.08	0.17	0.23	10.49
$C_{20}H_{20}N_4O_6SZn$	102.63	0.17	0.19	8.21
$C_{36}H_{26}N_8O_4S_2Zn$	114.98	0.17	0.19	9.20
Quinine Sulphate	777.95	–	–	54.00

CIE parameters

International commission on illumination (CIE) gave a set of parameters to estimate the colour of radiated light by a body. CIE coordinates are enumerated in Table 7. The colour coordinates of synthesized samples match well with bluish colour of National Television Standard Committee (NTSC: $x=0.14$, $y=0.08$) and European Broadcasting Union (EBU: $x=0.16$, $y=0.07$). CIE chromaticity diagrams (Fig. 6) were plotted from this data using colour calculator software. Observed colour coordinates and quantum yield values for copper complexes advocate their application in blue light emitting objects in several electroluminescent materials like OLEDs [58]. High quantum yield values of copper complexes also endorse above purpose.

Antimicrobial properties

The antibacterial and antifungal potential of synthesized samples was checked with respect to two Gram-positive, two Gram-negative, two fungal organisms as well as compared with standard drugs. The results have been shown in form of diameter of zone of inhibition in Table 8 and Fig. 7 for antibacterial screening and in Fig. 8 for mycelial % growth for antifungal screening. Solvent DMSO used in this study was also screened against all pathogens taken and did not exhibit any activity. Also, the metal salts used in this study did not exhibit any antibacterial potential against tested microorganisms. The compounds exhibited more activity against gram-positive bacteria than gram-negative bacteria. Pictorial representation of zone of inhibition of some of the

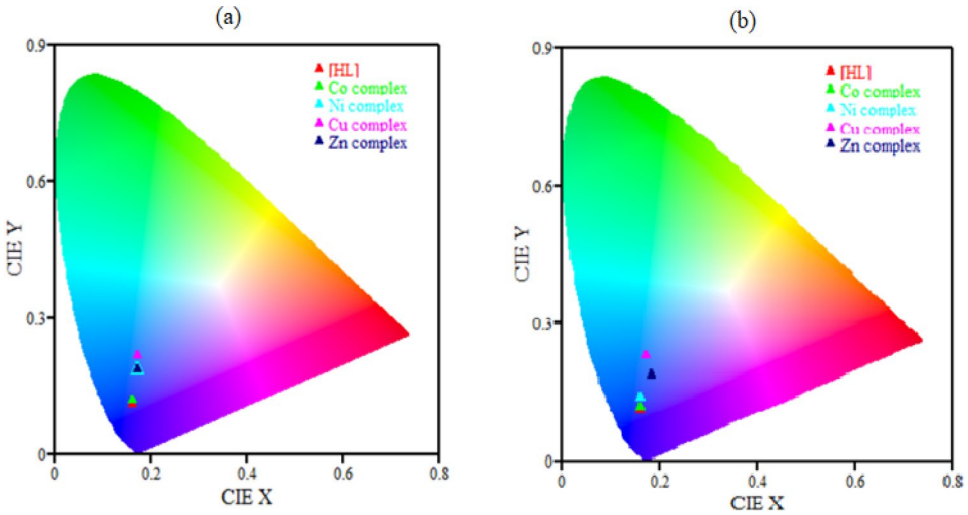

Fig. 6 Colour chromaticity representation of **a** ligand and 1:1 metal compounds **b** ligand and 1:2 metal compounds

Table 8 Antibacterial activity of synthesized compounds and standard drug sample

Compounds	Code	Diameter of growth of inhibition zone (mm)[c]			
		Gram-positive bacteria		Gram-negative bacteria	
		B. subtilis	*S. aureus*	*E. coli*	*P. aeruginosa*
Schiff Base	[HL]	–	–	–	–
$C_{20}H_{20}N_4O_6SCo$	Co–1	13.6	14.6	–	12
$C_{36}H_{26}N_8O_4S_2Co$	Co–2	12.8	11.3	–	12
$C_{20}H_{20}N_4O_6SNi$	Ni–1	11.2	12.6	–	12.3
$C_{36}H_{26}N_8O_4S_2Ni$	Ni–2	9	12.3	–	12
$C_{20}H_{16}N_4O_4SCu$	Cu–1	18.2	17.6	–	15
$C_{36}H_{22}N_8O_2S_2Cu$	Cu–2	18.1	16.6	–	14.6
$C_{20}H_{20}N_4O_6SZn$	Zn–1	22	19.3	18	18.3
$C_{36}H_{26}N_8O_4S_2Zn$	Zn–2	21.6	20.6	18	18.6
Ciprofloxacin	Ciprofloxacin	24	26.6	25	22

– = activity was not observed

[c]Values not including diameter of the well (8 mm) are means of three replicates

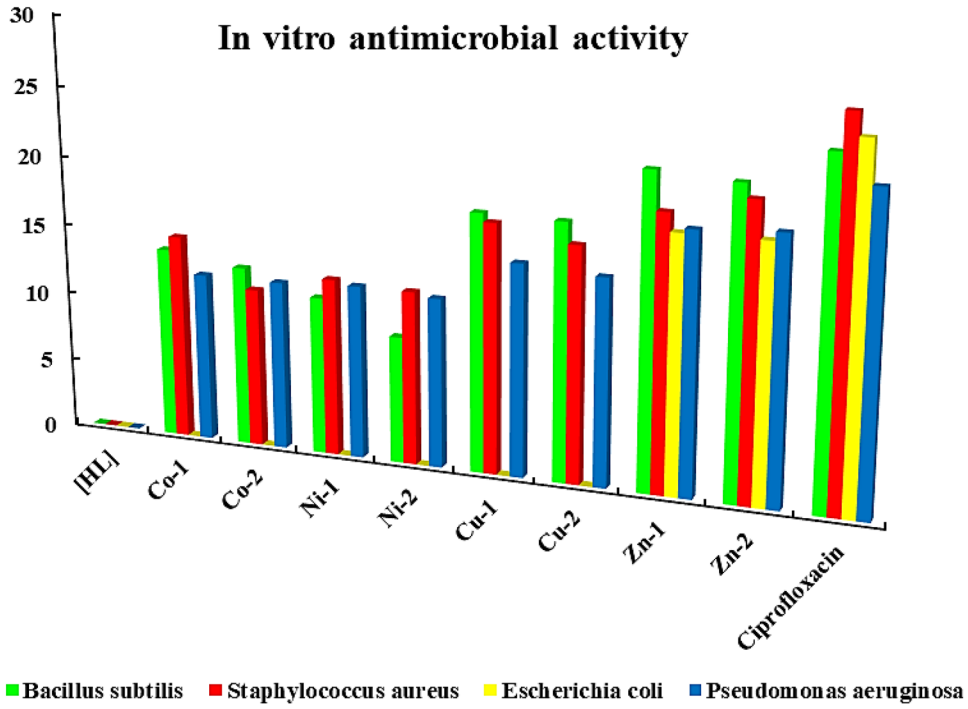

Fig. 7 Antibacterial activity of synthesized samples and standard drug

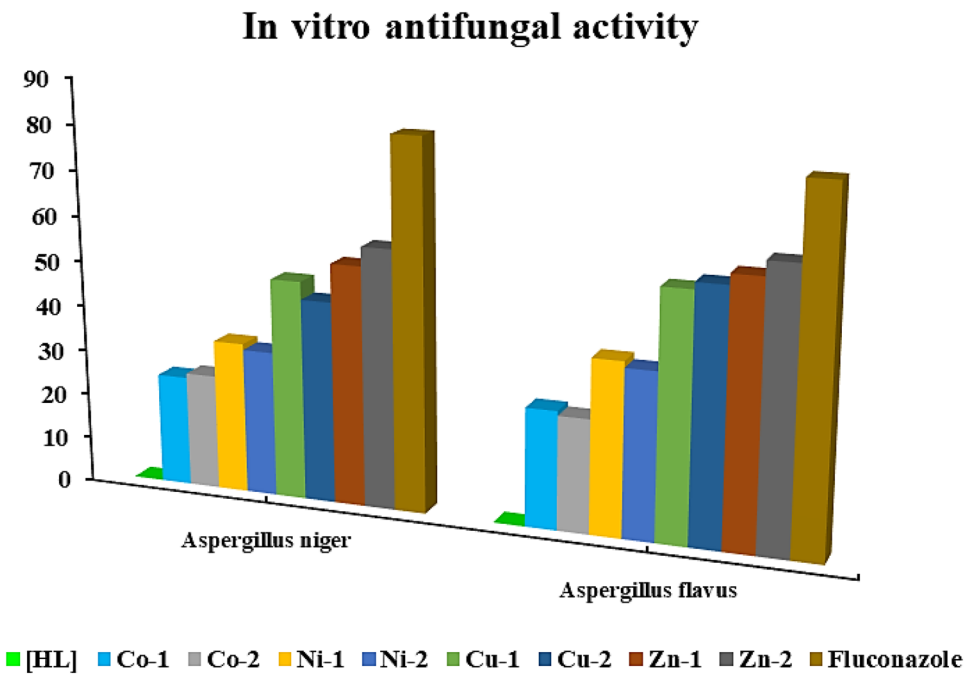

Fig. 8 Mycelial growth inhibition (%) of all samples and Fluconazole

metal complexes against these organisms are given in Fig. S12-S16 in supporting information.

A good antimicrobial molecule either effectively kills bacteria or slows down their speed of growth without being much toxic to tissues present in their close proximity. Such molecule may opt any of the two mechanisms; one is chemically interfering with synthesis of components of bacteria and other is to circumvent the mechanism of antimicrobial resistance. Antimicrobial agents can bind to the lipid-A component of lipopolysaccharide and cause alterations in structures, this will further result into fast destruction of bacterial cell membrane. Large hydrophobic moieties bind to the membrane proteins and change the permeability of the membranes.

The basis for this difference in sensitivity between compounds might be credited to the difference in morphological

constitutions of these microorganisms [47]. This can be explained due to the presence of lipopolysaccharides in outer phospholipidic membrane of Gram-negative bacteria cell wall which act as diffusion barrier for compounds making them less susceptible [59]. On the other hand, the Gram-positive bacteria are more susceptible due to comprising of only outer peptidoglycan layer which is not an effectual permeability obstruction. In spite of this permeability differences, some samples still exerted some degree of inhibition against Gram-negative bacteria as well. Individual metal ion plays its role in the antibacterial activity of metal complexes. The inhibitory potential of some of the tested compounds was found to be good as compared to that of reference drugs. All these findings show that antimicrobial activity not only depends on molecular structure of bacterial strains but also on the molecular structure of the tested compounds. MIC values of compounds are also shown in Fig. 9 (Table T1 in supporting information). Both copper and zinc complexes exhibit better antibacterial property than other compounds and these complexes are also better fungicidal with mycelial cell growth in range 44–61% against *A. niger* and *A. flavus* organisms. Antimicrobial properties of synthesized complexes were compared with other similar complexes. Outcomes of comparable study show that these complexes possess better activity towards bacterial strains and zinc complexes are more effective [24, 30, 60]. Structural moieties and nature of the central metal of these complexes form the basis of activity of these complexes. Advised structures of all metal chelates are shown in Fig. 10.

Conclusion

In summary, this paper describes the synthesis and spectroscopic characterization of a series of Co(II), Ni(II), Cu(II) and Zn(II) complexes with new Schiff base ligand derived from condensation of anthracene-10-carbaldehyde with 4-amino-3-mercapto-1,2,4-triazin-5(4*H*)-one. All the synthesized compounds have been characterized with the help of various physiochemical techniques. Thermal analysis and infrared spectral studies confirmed the presence of water molecules in coordination sphere of complexes. Thermal stability and kinetic factors were computed using Coats–Redfern method. Copper complexes are found to possess significant fluorescent properties with high quantum yield which endorse their uses in electroluminescent materials. Electrochemical studies of copper complexes indicate their redox behaviour. On the basis of analytical and spectral characterization, copper complexes are found to exhibit square planar structures and cobalt, nickel and zinc complexes are advised with octahedral geometries. All synthesized compounds have been investigated for antibacterial and antifungal activities. The inhibitory potential of some of tested compounds was found to be good against

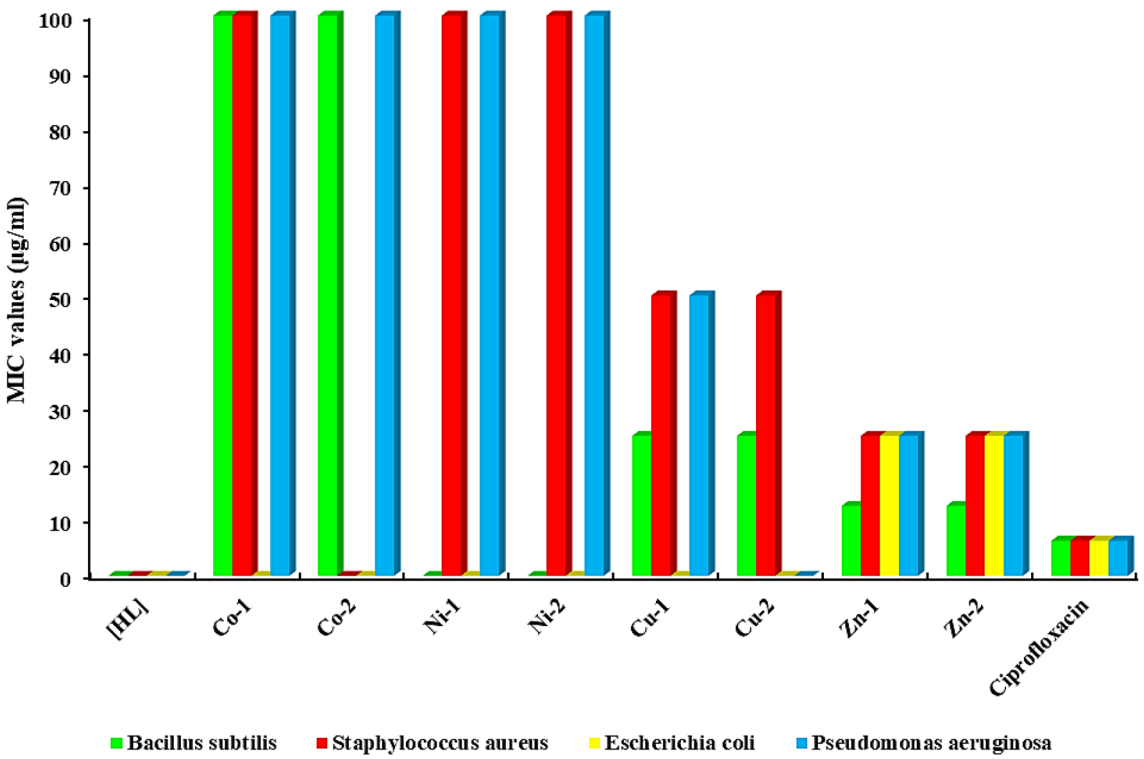

Fig. 9 MIC values comparison of synthesized samples with standard drug

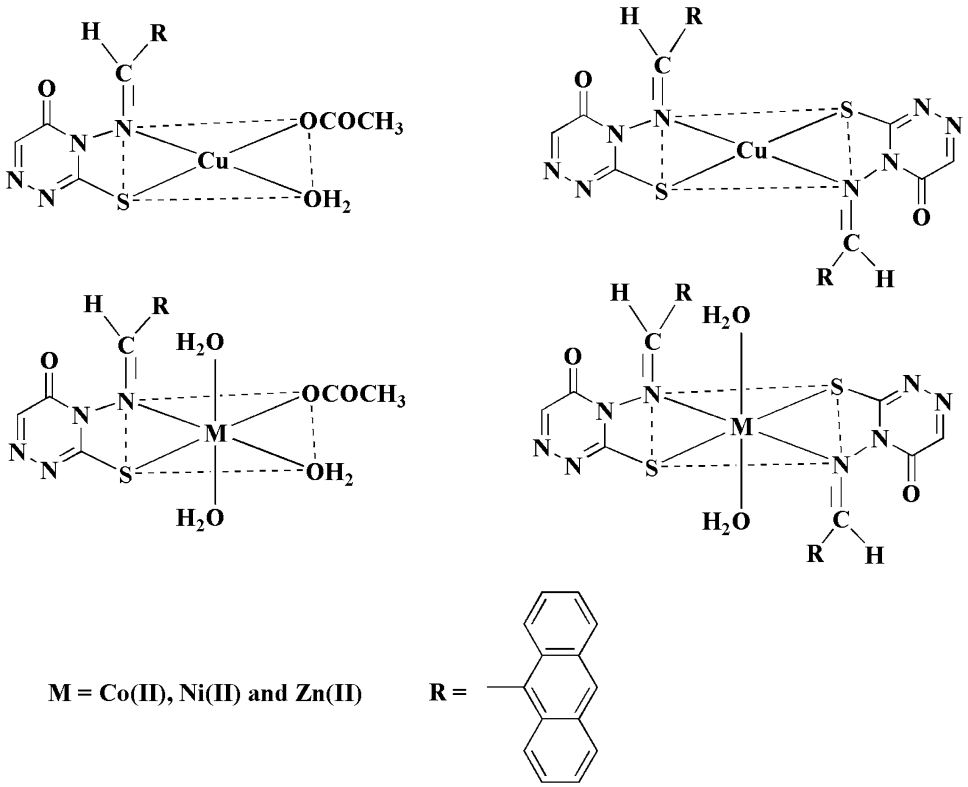

Fig. 10 Structures of metal complexes

some organisms. Zinc metal chelates have been found with more inducing ability to constrain the growth of bacterial and fungal species than other metal complexes and ligand.

Supplementary Information The online version contains supplementary material available at https://doi.org/10.1007/s13738-022-02567-y.

Acknowledgements We express genuine gratefulness to DST-FIST programme 2017 and Department of Chemistry, Kurukshetra University, Kurukshetra, for providing essential research facilities.

References

1. N.A.H. Alshammari, D.A. Bakhotmah, Polycycl. Aromat. Compd. (2022). https://doi.org/10.1080/10406638.2022.2025863
2. H.M. Diab, W.M.I. Hassan, I.A. Abdelhamid, A.H.M. Elwahy, J. Mol. Struct. (2019). https://doi.org/10.1016/j.molstruc.2019.07.047
3. B. Ramachandra, B. Narayana, Indian J. Chem. **38**, 1297 (1999)
4. K. Singh, P. Turk, A. Dhanda, Eur. Chem. Bull. (2018). https://doi.org/10.17628/ecb.2018.7.194-202
5. K. Singh, R. Thakur, V. Kumar, Beni-Suef Univ. J. Basic. Appl. Sci. (2016). https://doi.org/10.1016/j.bjbas.2016.02.001
6. M.A. Ibrahim, R.M. Abdel-rahman, A.M. Abdel-halim, S.S. Ibrahim, H.A. Allimony, ARKIVOC **16**, 202–215 (2008)
7. T.E. Ali, Eur. J. Med. Chem. (2009). https://doi.org/10.1016/j.ejmech.2009.06.022
8. Z. Zhang, Y. Zhang, D. Yao, H. Bi, I. Javed, Y. Fan, H. Zhang, Y. Wang, Crystal Growth Des. (2009). https://doi.org/10.1021/cg9008569
9. M. Barwiołek, M. Babinska, A. Kozakiewicz, A. Wojtczak, E. Szłyk, Polhedron (2017). https://doi.org/10.1016/j.poly.2017.06.019
10. D. Sek, M. Siwy, M. Grucela, G. Małecki, E.M. Nowak, G. Lewinska, J. Santera, K. Laba, M. Lapkowski, S. Kotowicz, E. Schab-Balcerzak, Spectrochim. Acta Part A Mol. Biomol. Spectrosc. (2017). https://doi.org/10.1016/j.saa.2016.12.013
11. R. Kalarani, M. Sankarganesh, G.G.V. Kumar, M. Kalanithi, J. Mol. Struct. (2020). https://doi.org/10.1016/j.molstruc.2020.127725
12. Z. Kazemi, Z. Chavoshpour-natanzi, V. Mirkhani, Inorganica Chim. Acta. (2020). https://doi.org/10.1016/j.ica.2020.120004
13. H. Kargar, R. Behjatmanesh-ardakani, V. Torabi, M. Kashani, Polyhedron (2021). https://doi.org/10.1016/j.poly.2020.114988
14. H. Kargar, V. Torabi, A. Akbari, R. Behjatmanesh, A. Muhammad, N. Tahir, J. Iran. Chem. Soc. (2019). https://doi.org/10.1007/s13738-018-01583-1
15. H. Kargar, F. Aghaei-meybodi, M.R. Elahifard, M.N. Tahir, M. Ashfaq, K. Shahzad, J. Coord. Chem. (2021). https://doi.org/10.1080/00958972.2021.1900831
16. M. Fallah-mehrjardi, H. Kargar, R. Behjatmanesh-ardakani, J. Mol. Struct. (2022). https://doi.org/10.1016/j.molstruc.2021.132037
17. N.K. Gondia, S.K. Sharma, Opt. Quantum Electron. (2017). https://doi.org/10.1007/s11082-017-1138-9
18. D. Majumdar, D. Das, S.S. Sreejith, S. Das, J. Kumar, Inorganica Chim. Acta (2019). https://doi.org/10.1016/j.ica.2019.02.022
19. Y. Pan, Y. Zhang, L. Wang, Appl. Organomet. Chem. (2020). https://doi.org/10.1002/aoc.5441
20. H. Kargar, A. Adabi, M. Nawaz, M. Ashfaq, K. Shahzad, J. Mol. Struct. (2021). https://doi.org/10.1016/j.molstruc.2021.130112
21. H. Kargar, A. Adabi, A. Khurram, S. Munawar, M. Ashfaq, J. Iran. Chem. Soc. (2021). https://doi.org/10.1007/s13738-021-02207-x

22. H. Kargar, F. Aghaei-meybodi, R. Behjatmanesh-ardakani, J. Mol. Struct. (2021). https://doi.org/10.1016/j.molstruc.2021.129908
23. H. Kargar, A. Adabi, M. Nawaz, M. Ashfaq, K. Shahzad, J. Mol. Struct. (2021). https://doi.org/10.1016/j.molstruc.2020.129842
24. H. Kargar, M. Fallah-mehrjardi, R. Behjatmanesh-ardakani, H. Amiri, A. Adabi, S. Sedighi-khavidak, K. Shahzad, M. Ashfaq, M. Nawaz, Inorganica Chim. Acta (2022). https://doi.org/10.1016/j.ica.2021.120677
25. H. Kargar, M. Fallah-mehrjardi, M. Ashfaq, K. Shahzad, M.N. Tahir, R. Behjatmanesh-ardakani, A. Rudbari, A.A. Ardakani, S. Sedighi-khavidak, J. Coord. Chem. (2021). https://doi.org/10.1080/00958972.2021.1990271
26. M. Heidelberger, H.P. Treffers, J. Gen. Physiol. (1942). https://doi.org/10.1085/jgp.25.4.523
27. A.S. Ramasubramanian, B. Ramachandra Bhat, R. Dileep, J. Rasayan, Chem **3**, 122 (2010)
28. C.J. Dhanaraj, M.S. Nair, J. Coord. Chem. (2009). https://doi.org/10.1080/00958970903191142
29. A.A. Pawanoji, B.H. Mehta, Asian J. Chem. **21**, 6869 (2009)
30. A. Sahraei, H. Kargar, M. Hakimi, M.N. Tahir, J. Mol. Struct. (2017). https://doi.org/10.1016/j.molstruc.2017.08.022
31. A. Gubendran, G. Gangatharan, V. Kumar, M. Palsamy, K. Gurusamy, R. Periakaruppan, Appl. Organomet. Chem. (2017). https://doi.org/10.1002/aoc.4128
32. K. Singh, D.P. Singh, M. SinghBarwa, P. Tyagi, Y. Mirza, J. Enzyme, Inhib. Med. Chem. (2006). https://doi.org/10.1080/14756360600838648
33. C.C.R. Sutton, G. Da Silva, G.V. Franks, Chem. A Eur. J. (2015). https://doi.org/10.1002/chem.201406516
34. K. Singh, S. Raparia, P. Surain, Med. Chem. Res. (2015). https://doi.org/10.1007/s00044-014-1298-0
35. S.H. Sumrra, M. Ibrahim, S. Ambreen, M. Imran, M. Danish, F.S. Rehmani, Bioinorg. Chem. Appl. (2014). https://doi.org/10.1155/2014/812924
36. K. Singh, P. Turk, A. Dhanda, Appl. Organomet. Chem. (2021). https://doi.org/10.1002/aoc.6088
37. A.A. Ardakani, H. Kargar, N. Feizi, M.N. Tahir, J. Iran. Chem. Soc. (2018). https://doi.org/10.1007/s13738-018-1347-6
38. A.S. Munde, A.N. Jagdale, S.M. Jadhav, T.K. Chondhekar, J. Serbian Chem. Soc. (2010). https://doi.org/10.2298/JSC090408009M
39. B.J. Hathaway, D.E. Billing, Coord. Chem. Rev. (1970). https://doi.org/10.1016/S0010-8545(00)80135-6
40. M.B. Fugu, N.P. Ndahi, B.B. Paul, A.N. Mustapha, J. Chem. Pharm. Res. **5**, 22 (2013)
41. B. Geeta, K. Shravankumar, P.M. Reddy, E. Ravikrishna, M. Sarangapani, K.K. Reddy, V. Ravinder, Spectrochim. Acta Part A Mol. Biomol. Spectrosc. (2010). https://doi.org/10.1016/j.saa.2010.08.004
42. N. Kavitha, P.V. AnanthaLakshmi, J. Saudi, Chem. Soc. (2017). https://doi.org/10.1016/j.jscs.2015.01.003
43. A.B.P. Lever, D. Ogden, Inorg. Phys. Theor. **2041**, 2 (1965)
44. G. Lupașcu, E. Pahonțu, S. Shova, ȘF. Bărbuceanu, M. Badea, C. Paraschivescu, J. Neamțu, M. Dinu, R.V. Ancuceanu, D. Drăgănescu, C.E. Dinu-Pîrvu, Appl. Organomet. Chem. (2021). https://doi.org/10.1002/aoc.6149
45. M.P. Kesavan, G.G. VinothKumar, J. DhaveethuRaja, K. Anitha, S. Karthikeyan, J. Rajesh, J. Photochem Photobiol B Biol (2017). https://doi.org/10.1016/j.jphotobiol.2016.11.024
46. Y. Abdi, N. Bensouilah, D. Siziani, M. Hamdi, A.M.S. Silva, B. Boutemeur-Kheddis, J. Mol. Struct. (2020). https://doi.org/10.1016/j.molstruc.2019.127307
47. M. Gaber, N. El-Wakiel, K. El-Baradie, S. Hafez, J. Iran. Chem. Soc. (2019). https://doi.org/10.1007/s13738-018-1494-9
48. A. Abayneh, T. Gebretsadik, S. Tadesse, M. Thomas, Adv. Chem. Engineer. Sci. (2018). https://doi.org/10.4236/aces.2018.84017
49. W. Benabid, K. Ouari, S. Bendia, R. Bourzami, M.A. Ali, J. Mol. Struct. (2020). https://doi.org/10.1016/j.molstruc.2019.127313
50. N. Özpozan, H. Arslan, T. Özpozan, M. Merdivan, N. Külcü, J. Therm. Anal. Calorim. (2000). https://doi.org/10.1023/A:1010171230450
51. S.M. Emam, D.A. Tolan, A.M. El-Nahas, Appl. Organomet. Chem. (2020). https://doi.org/10.1002/aoc.5591
52. S.M. Alshehri, A. Al-Fawaz, T. Ahamad, J. Anal. Appl. Pyrolysis. (2013). https://doi.org/10.1016/j.jaap.2013.01.004
53. M. Serhan, M. Sprowls, D. Jackemeyer, M. Long, I.D. Perez, W. Maret, N. Tao, E. Forzani, AIChE Annu., Meet. Conf. Proc. (2019). https://doi.org/10.1039/x0xx00000x
54. R.D. Costa, E. Ortí, H.J. Bolink, F. Monti, G. Accorsi, N. Armaroli, Angew. Chemie - Int. Ed. (2012). https://doi.org/10.1002/anie.201201471
55. S. Densil, C. Huei, C. Chia, L. Chen, A. Mathavan, V. Sathish, P. Thanasekaran, A. Ramdass, W.S. Li, Luminiscence (2018). https://doi.org/10.1002/bio.3477
56. N.K. Gondia, S.K. Sharma, Mater. Chem. Phys. (2019). https://doi.org/10.1016/j.matchemphys.2018.12.014
57. B. Brandner, Implementation of a Comparative Method for Measuring Photoluminescence Quantum Yields of Novel Compounds in Solution. (Oregon State University, 2016) https://ir.library.oregonstate.edu/concern/undergraduate_thesis_or_projects/8336h352k. Accessed 21 July 2017
58. L. Subha, C. Balakrishnan, S. Natarajan, M. Theetharappan, B. Subramanian, M.A. Neelakantan, Spectrochim. Acta A Mol. Biomol. Spectrosc. (2015). https://doi.org/10.1016/j.saa.2015.08.033
59. S. Yordanova, H.T. Temiz, I.H. Boyaci, S. Stoyanov, E. Vasileva-Tonkova, A. Asiri, I. Grabchev, J. Mol. Struct. (2015). https://doi.org/10.1016/j.molstruc.2015.08.012
60. A. Sahraei, H. Kargar, M. Hakimi, M. Nawaz, Transit. Met. Chem. (2017). https://doi.org/10.1007/s11243-017-0152-x